JCTC Journal of Chemical Theory and Computation

Article

pubs.acs.org/JCTC

Carotenoids and Light-Harvesting: From DFT/MRCI to the Tamm–Dancoff Approximation

Oliviero Andreussi,*[,†] Stefan Knecht,[‡] Christel M. Marian,[§] Jacob Kongsted,[∥] and Benedetta Mennucci*[,†]

[†]Dipartimento di Chimica e Chimica Industriale, University of Pisa, Via G. Moruzzi, 56124 Pisa, Italy

[‡]Laboratory of Physical Chemistry, ETH Zürich, Vladimir-Prelog-Weg 2, 8093 Zürich, Switzerland

[§]Institute of Theoretical and Computational Chemistry, University of Düsseldorf, Universitaïsstraße 1,40225 Düsseldorf, Germany

[∥]Department of Physics, Chemistry and Pharmacy, University of Southern Denmark, Campusvej 55, 5230 Odense M, Denmark

Supporting Information

ABSTRACT: Carotenoids are known to play a fundamental role in photosynthetic light-harvesting (LH) complexes; however, an accurate quantum-mechanical description of that is still missing. This is due to the multideterminant nature of the involved electronic states combined with an extended conjugation which limits the applicability of many of the most advanced approaches. In this study, we apply a multireference configuration interaction extension of density functional theory (DFT/MRCI) to describe transition energies and densities as well as the corresponding excitonic couplings, for the three lowest singlet excited states of nine carotenoids present in three different LH complexes of algae and plants. These benchmark results are used to find an approximated computational approach, which could be used to quantitatively reproduce the key quantities at a reduced computational cost. To this end, we tested the Tamm–Dancoff approximation (TDA) to time-dependent density functional theory in combination with different functionals. By analyzing the errors with respect to DFT/MRCI-TDA results for the full set of electronic properties, we conclude that TDA-TPSS with small basis sets indeed represents an effective approach to investigate LH processes that involve carotenoids.

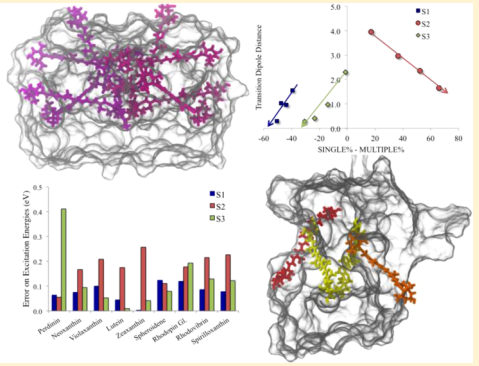

1. INTRODUCTION

In order to optimize the spectral cross-section for photosynthetic activity, many organisms have supplemented the normal "antenna" pigments in their light-harvesting (LH) complexes, the (bacterio)chlorophylls ((B)Chl), with another type of pigments, the carotenoids (Cars).[1,2] Carotenoids, in fact, absorb light in a spectral region not accessible to (B)Chls.[3] As both carotenoids and (B)Chls can contribute with various close-lying excited states, many different pathways of energy transfer are possible among the two sets of pigments.[1,4,5] Moreover, these paths can represent energy transfer from carotenoids to (B)Chl and vice versa. The former path is the common one in the LH process while the latter plays a fundamental role in photoprotective quenching mechanisms.[6−9]

Cars are known to primarily involve the two lowest of their excited states in the energy transfer processes. The nature of these two states is generally represented using an ideal picture of a π-system in a perfect C_{2h} symmetry:[10,11] according to this model, the lowest lying singlet state (S1) is described by the same irreducible representation as the ground state (A_g^-) while the second singlet excited state (S2) state has B_u^+ symmetry. An additional dark B_u^- state termed S3 is also predicted by the model. This analysis implies that the S0 → S1 transition is (electric dipole) forbidden and the lowest state, which is accessible through light absorption, is S2. The S1 state can thus be populated mainly by internal conversion from S2: experimental evidence shows that this internal conversion is generally fast[3,12] (on a sub-200 fs time scale) and can be very competitive with respect to the transfer process to the (B)chlorophylls making the S1 to (B)Chl pathway possible. Which state contributes most to the transfer depends on its relative position with respect to the (B)Chls states, predominantly the (B)Chl Q_x and Q_y states. The relative energy of the carotenoids states are in fact largely dependent on the conjugation length[11] and for Cars with nine or more conjugated double bonds, the presence of another dark state lying between the S1 and S2 states has also been suggested by experiments.[13−17] This state has been interpreted either as a separate electronically excited state, an excited-state isomer, a vibrationally hot ground state, a consequence of different ground state isomers,[18] or as the result of chemical impurities.[19]

In spite of many years of studies, the exact mechanism of energy transfer from Cars to (B)Chls remains controversial, owing especially to the complex electronic structure of Cars. What is known is that the pathway from S2 is active in almost all LH systems, while the S1 route strongly depends on the

Received: December 13, 2014
Published: January 15, 2015

DOI: 10.1021/ct5011246
J. Chem. Theory Comput. 2015, 11, 655−666

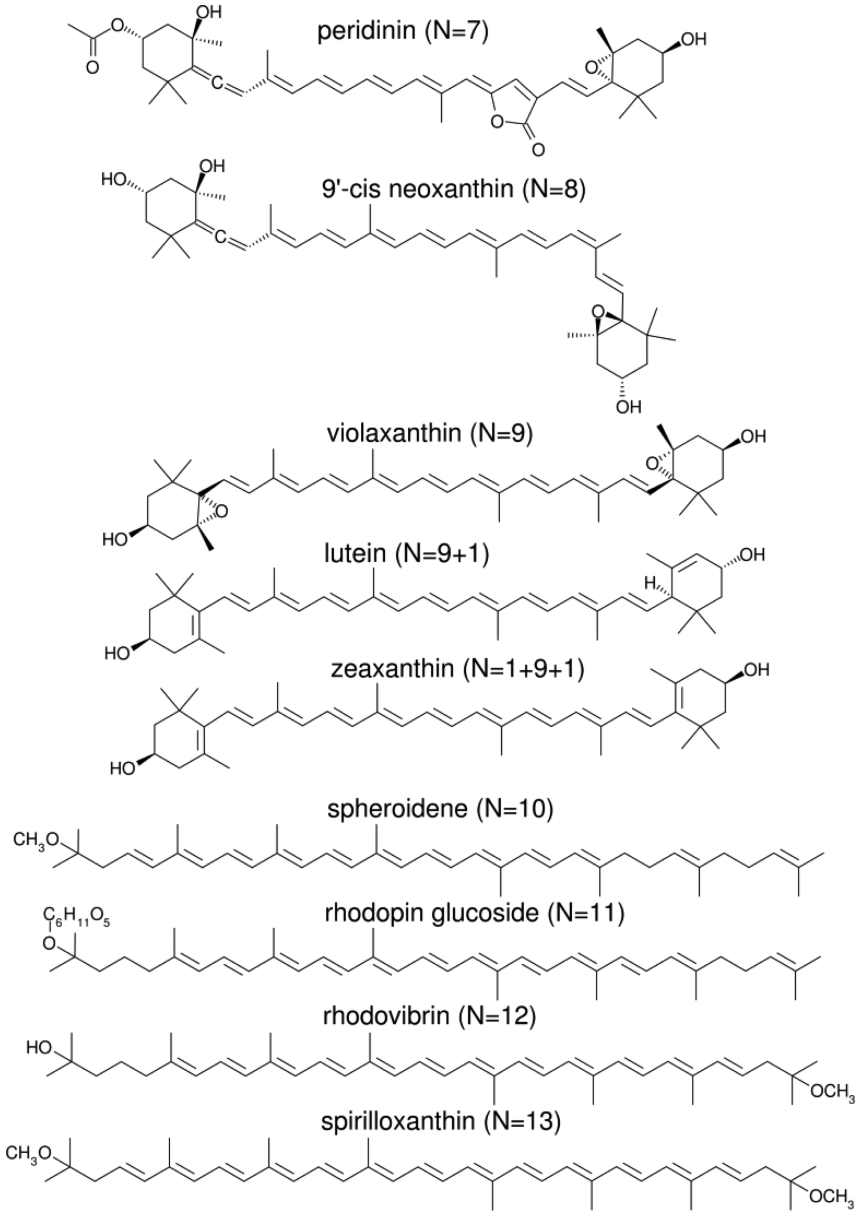

Figure 1. Chemical structure of the full set of nine carotenoids analyzed in the present study, in order of increasing conjugation length (N).

specific carotenoid, as the S1 energy can go below the lowest (Q_y) state of (B)Chls.[1,3] Thus, the relative position of the S2 and S1 energies with respect to those of (B)Chl states is the "key" aspect for optimizing the overall efficiency of energy transfer. Unfortunately, a detailed description of the Cars electronic states with quantum-mechanical (QM) approaches is still a challenge due to the multireference character of some of these states combined with the size of the systems, which prevents the use of very accurate and highly correlated methods. It is known, that the various excited states have a rather different multireference character,[10,11,20,21] S2 being largely dominated by a single excitation while S1 (and S3) present strong double excitation characters possibly mixed with single excitations. As a result, single-reference approaches only properly describe S2 (which becomes the lowest singlet state) while they cannot give the correct energy position and character of, for example, the S1 state.

So far, most calculations on these states rely either on semiempirical[10,11,20,22−25] (SE) or time-dependent density functional[26−28] (TD-DFT) formulations. In the former case, the multireference (MR) aspect can partly be accounted for but with the disadvantage of a SE description, while in the latter a more accurate description of the electron density can be achieved but misses the MR aspect, since the exact functional is unknown. Surprisingly, TD-DFT and in particular its Tamm−Dancoff approximation (TDA) can yield a lowest excited state with a dark S1-like character when combined with specific DFT functionals and basis sets. This unexpected behavior has been explained by a fortuitous cancellation of errors:[21] considering linear all-trans polyenes of increasing length, Starcke et al.[21] have shown that the importance of double excitations grows faster for the ground state than for the excited states, and the result is that the errors caused by the neglect of double excitations in the ground and excited states will match at some point. For this reason, the error of the S1(A_g^-) excitation energies at the TDA level decreases with increasing number of double bonds, while the error in the singly excited S2(B_u^+) state is essentially independent of the chain length. For the S3(B_u^-)

DOI: 10.1021/ct5011246
J. Chem. Theory Comput. 2015, 11, 655−666

state, a behavior similar to the S1 state can be expected, since doubles are here as important as for the S1 state.

A possible, effective strategy to go beyond (the application range of) TD-DFT is that of using the DFT/MRCI ansatz developed by Grimme and co-workers.[29] This method has been applied to study excited-state properties of Cars by several groups.[4,17,29−34] Recently, some of the authors have applied the DFT/MRCI approach to the study[31] of the lowest singlet excited states of a specific carotenoid, namely peridinin, present in the PCP light-harvesting system of dinoflagellates. Peridinin is a unique example of a carotenoid, as it contains a conjugated carbonyl group, which makes its spectroscopic features more dependent on the environment as compared to other Cars, due to its more polar character as well as the possibility of hydrogen-bonding interactions through the carbonyl oxygen.[35] In that DFT/MRCI study,[31] a distinct dependence of the relative energy position of the two lowest excited states on the bond-length alternation (which can be modified by the environment) was shown with a clear indication that this tuning was caused by a change of the nature of each excited state along with its multireference character. A related investigation on effect of the geometry on peridinin excitations has been recently presented by Coccia et al. using a Variational Monte Carlo approach.[36] Here, we extend the DFT/MRCI benchmarking analysis to a set of eight different Cars with variable conjugation length and composition (see Figure 1). Four of them (neoxanthin, violaxanthin, zeaxanthin, and lutein) belong to the family of oxygenated Cars called xantophylls. Xanthophylls are the typical yellow pigments of leaves while the other four Cars (spheroidene, rhodopin glucoside, rhodovibrin, and spirilloxanthin) belong to the family of Cars present in bacteria.

The goal of the present study is twofold. First of all, we aim at obtaining a benchmark description of the electronic parameters to be used in the modeling of the light-harvesting (and photoprotection) functionalities of pigment−protein complexes. These parameters are the excitation properties of the pigments (transition energies and transition dipoles) and the interactions among them (i.e., the electronic couplings). To achieve the first objective, we analyze transition energies together with transition densities (from which the electronic couplings are obtained) for the three lowest singlet excited states of the nine carotenoids reported in Figure (1) using a DFT/MRCI approach. The second objective is to investigate the possibility of finding a computationally cheaper yet reliable approach, which could be proposed for applications on real natural light-harvesting complexes. To achieve this second objective, we assess the performance of the TDA approach (coupled to different DFT functionals) with respect to both transition energies and transition densities by comparison to the DFT/MRCI results. DFT/MRCI has in fact shown to be a reliable approach to study relative energies of long polyenes: the absolute values of the excitation energies are known to be underestimated but of the same magnitudes for all the three states.[29] On the contrary, an accurate estimation of these energies from experiments faces various difficulties. The first difficulty is obviously to determine the energetic location of the dark states. As a matter of fact, even for the bright state, it is by no means trivial to extract "vertical" excitation energies from the spectra that typically show a vibronic structure. Another reason is the strong solvent dependence of the absorption, which leads to substantial scatter in the experimental data.

This paper is organized as follows: after a description of the computational details (Section 2), we report benchmark calculations using DFT/MRCI and analyze the aforementioned properties of the first three excited states with respect to the conjugation length of the carotenoids (Section 3). Then, we proceed with the analysis of the performances of the TDA approach, starting from the convergence of the excitation properties with respect to the basis set for two geometries of one selected carotenoid (Section 4). For the same two systems, a first screening of different density functionals is performed and a subset of functionals that show promising performances is extracted (Section 4). Results on the larger set of carotenoids obtained with TDA using the best functional are then compared to DFT/MRCI calculations (Section 5). We conclude with an analysis of the range of validity and the estimated accuracy of TDA calculations when applied to the estimation of electronic couplings for clusters of the same carotenoids present in natural light-harvesting systems.

2. COMPUTATIONAL DETAILS

The DFT/MRCI calculations were carried out as single-point calculations at the DFT-geometry optimized structures (*vide infra*) using a parallel version of the DFT/MRCI program.[29,30] Our present setup is along similar lines of the computational recipe that we successfully applied in our previous work on peridinin.[31] A split valence basis set (def2-SV(P))[37] that contains a d-polarization function on all non-hydrogen atoms was used for all atom types. The Kohn−Sham (KS) orbitals were optimized using the BH-LYP functional[38,39] as implemented in the Turbomole 6.3 program package.[40] These orbitals define the basis for the construction of the configuration state functions in the MRCI expansion. Keeping the 1s electrons of the heavy atoms frozen in the post-SCF steps, the initial MRCI reference space was spanned by all single and double excitations from the six highest occupied MOs to the five lowest unoccupied MOs of the ground state KS determinant. We chose an orbital selection threshold of 0.6 E_h to compute the lowest 12 eigenvectors. The new reference space for the second DFT/MRCI step then comprised all configurations contributing to one of the 12 lowest-lying eigenvectors of the initial DFT/MRCI calculation with a squared coefficient of 0.003 and larger. At this stage, we optimized the ground and lowest seven electronically excited states of the target carotenoid.

All geometry optimizations and TDA calculations were performed with a development version of Gaussian.[41] The structures of the nine Cars have been optimized in the ground state (@GS) using the hybrid B3LYP functional.[38,39] For peridinin, a second geometry (@EXC) has been investigated, namely the one referring to the lowest bright excited state (S2 according to the previous nomenclature), as obtained using the CAM-B3LYP[42] functional. Both structures of peridinin were taken from our previous work[31] and were obtained via geometry optimization in vacuo with the 6-31G(d) basis set. The same basis set was used for the optimization of spheroidene, rhodopin-glucoside, rhodovibrin, and spirilloxanthin, while the structures of the four xantophylls (lutein, neoxanthin, violaxanthin, and zeaxanthin) were taken from ref 43 and were obtained using the triple-ζ 6-311G(d) basis set.

Basis set effects have been estimated by comparison of the results obtained using the 6-31g(d) and 6-31+g(d) basis sets compared to the 6-311+g(d) basis set. Test calculations were also performed with Dunning's (triple-ζ) cc-pVTZ basis set[44]

DOI: 10.1021/ct5011246
J. Chem. Theory Comput. 2015, 11, 655−666

but revealed no significant differences with respect to the 6-311+g(d) basis set. However, more than one-third of the considered functionals failed to yield convergence at the SCF step with this larger basis set even when using a quadratic convergence solver.

In assessing the performance of TDA with different exchange-correlation functionals a total of 19 functionals were considered, comprising the most common classes available. The set includes the standard LDA and GGA (PBE,[45,46] PW91,[47−50] HCTH[51]) functionals, meta-GGA (TPSS,[52] RevTPSS,[53,54] VSXC,[55] M11L,[56,57] and MN12L[58]), hybrid meta-GGA (TPSSh,[52] BMK,[59] M05,[60] M06[61]), hybrids (B3LYP,[38,39] BHandH,[62] HSE06,[63−67] PBE0[68]), and long-range corrected functionals (CAM-B3LYP,[42] LC-wPBE[69−71]).

3. DFT/MRCI RESULTS

In this section, we summarize the main properties of the lowest three excited states of the nine different carotenoids (see Figure 1) calculated with the DFT/MRCI approach as described in Section 2. In Table 1, we report transition energies and transition dipoles of the three lowest excited states of the nine carotenoids calculated at their respective B3LYP ground state (GS) geometry. The Cars are reported in order of increasing conjugation length as presented in Figure 1.

Table 1. DFT/MRCI Transition Energies (in eV) and Transition Dipoles (au) of the first Three Excited States (S1−S3) of the Considered Carotenoids[a]

	S1		S2		S3	
carotenoid	*E* (eV)	TrDip (au)	*E* (eV)	TrDip (au)	*E* (eV)	TrDip (au)
peridinin	2.26	2.239	2.54	7.124	3.10	0.313
neoxanthin	2.26	0.254	2.61	7.758	2.98	0.797
violaxanthin	2.18	0.082	2.62	7.733	2.90	1.297
lutein	2.13	0.302	2.51	7.848	2.83	1.369
zeaxanthin	2.11	0.212	2.48	7.727	2.75	1.043
spheroidene	1.96	0.665	2.39	8.212	2.66	1.297
rhodopin-Gl	1.83	0.106	2.29	8.276	2.45	3.322
rhodovibrin	1.75	0.246	2.22	7.994	2.35	4.769
spirilloxanthin	1.66	0.042	2.12	7.458	2.23	6.289

[a]The carotenoids are ordered by increasing conjugation length.

As expected, for all the carotenoids the first two excitations correspond to small/large transition dipoles, respectively. The only exception is peridinin for which the lowest excitation is characterized by a rather large transition dipole. The properties of the third excited state are, on the contrary, very dependent on the conjugation length: the longer the conjugation length the more significant is the transition dipole, which almost equals the one corresponding to the "bright" (S2) excitation for spirilloxanthin. The corresponding excitation energies decrease as the conjugation length increases for all three excited states (with the second excited state of peridinins being an exception). Energies of the first excited state decrease more rapidly than the second one. Similarly, energies of the third excited state decrease more rapidly than those of S1 and S2. The net result of these different trends is that the second excited state is closer in energy to the first one only for peridinin, while it is equidistant from the first and third states for neoxanthin, and gets closer and closer to the third state as the conjugation length increases. The upper panel of Figure 2 illustrates this behavior, together with the parallel trend in the oscillator strengths (lower panel of Figure 2).

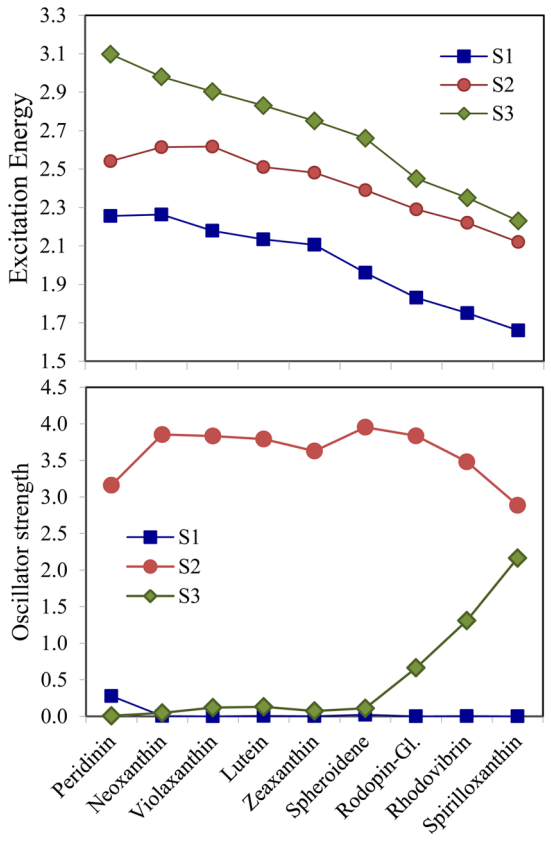

Figure 2. DFT/MRCI excitation energies and oscillator strengths of the nine Cars considered. All excitation energies are given in eV.

These results found for the transition energies and dipoles are mirrored by the associated oscillator strengths. In particular, all considered carotenoids exhibit a similar behavior in terms of oscillator strengths, with the second excited state showing the strongest value, while the third and, especially, the first excited states have negligible oscillator strengths in most cases. The third excitation, however, gains a significant intensity as the conjugation length increases. Note that peridinin is the only carotenoid that has a nonzero oscillator strength for the first excited state. Both findings are a result of a mixing of the second state with its neighboring states, the first one for peridinin or the third one for carotenoids with larger conjugation lengths. In order to gain further insight into the nature of the different excited states of the considered systems, we analyzed the percentages of single and multiple (double, triple, and quadruple) excitations for each state. The results are reported in order of increasing conjugation length of the carotenoids in Figure 3.

While the S2 state is clearly dominated by single excitations, contributions from multiple excitations are crucial for the first and third excited states. The trends reported above for excitation energies and oscillator strengths are well described in terms of singles vs doubles excitations. As reported previously,[31] at the present geometry, the S1 state of peridinin is characterized by a significantly larger (smaller) contribution of single (double) excitations, which is in turn responsible for the larger oscillator strength of this state compared to the remaining Cars. While no obvious trends can be observed for

DOI: 10.1021/ct5011246
J. Chem. Theory Comput. 2015, 11, 655−666

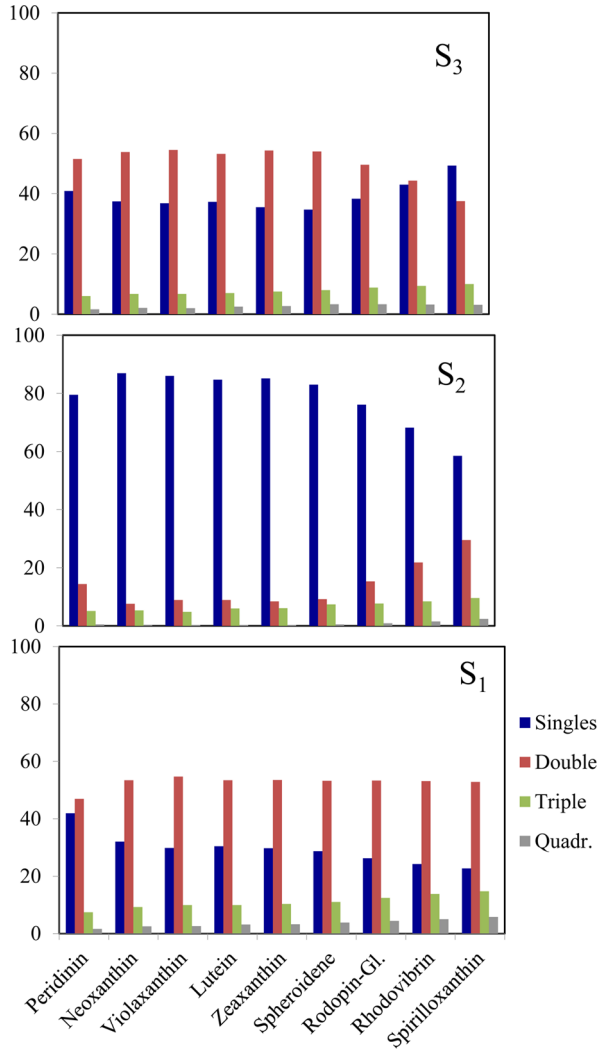

Figure 3. Decomposition of the lowest three excited states of Cars into single, double and higher order excitations. Results are reported as percentage contributions.

carotenoids with intermediate conjugation lengths, a more clear behavior is seen for longer carotenoids: considering the S2 state, the contribution of single (double) excitations decreases (increases) as the conjugation length increases, whereas the opposite trend is observed for the S3 state. Excitations higher than doubles seem to become more and more important as the conjugation length increases as indicated by their larger contribution to the S1 state of the longest carotenoids.

The analysis presented so far clearly suggests that all investigated Cars present the same picture in terms of the two lowest states, the first being always "dark" (with the exception of peridinin for which the S1 has a significant transition dipole) and the second being always bright. Differences among the Cars become instead evident if we also take into account the third excited state: in fact, its relative position and nature change significantly with the conjugation length. In particular, for the longer Cars we observe a clear mixing of this state with S2 that leads to a decrease of its excitation energy and a parallel increase of the transition dipole (and oscillator strength). For the longest Car, spirilloxanthin, the two states become almost degenerate with a very similar transition dipole. We note that in a previous study on β-carotene[17] it has been shown that by relaxing the excited state geometries, an inversion of S2 and S3 states can also be found.

To complete this picture, we also observe that the ground state of all Cars presents a non-negligible multideterminant component (from 13% to 20%), which increases with the conjugation length reaching about 20% in spirilloxanthin.

4. SCREENING OF BASIS SET AND DFT FUNCTIONAL

Moving to the investigation of the TDA approach, two aspects, namely the basis set and the DFT functional, have to be preliminarily analyzed before we can proceed with a comparison to the DFT/MRCI results. For this preliminary analysis, we have focused on a single Car, the peridinin which can be seen as the most "difficult" case as, in addition to the long conjugation, it also contains polar groups along the chain. Basis set effects have been analyzed by comparing the results for excitation energies and oscillator strengths for two different geometries (@GS and @EXC, see Computational Details). We compared the properties of the lowest three excited states using both geometries by taking the absolute deviation of the results with respect to the calculations performed using the largest basis set. Results, averaged over the different functionals, are summarized in Table 2 (see Supporting Information for the full set of data).

Table 2. Mean Absolute Errors (MAE) on Excitations Energies and Oscillator Strengths of the Lowest Three Excited States of Peridinin @GS and @EXC, Averaged over the Different Density Functionals Adopted in the TDA[a]

	MAE on excitation energies (eV)		MAE on oscillator strengths (au)	
	6-31G(d)	6-31+G(d)	6-31G(d)	6-31+G(d)
S1 @GS	0.015	0.002	0.19	0.03
S2 @GS	0.028	0.039	0.66	0.07
S3 @GS	0.055	0.016	0.53	0.05
S1 @EXC	0.011	0.002	0.16	0.03
S2 @EXC	0.066	0.003	1.62	0.10
S3 @EXC	0.052	0.013	1.48	0.07

[a]Errors are computed with respect to calculations performed with the 6-311+G(d) basis set. Only the density functionals among the selected 19 that showed convergence with the 6-311+G(d) basis set are considered in this analysis.

As expected, the calculations performed with the smallest basis set, which does not include diffuse functions, are not fully converged. On the contrary, the intermediate basis set (6-31+G(d)) is seen to perform almost as well as the valence triple-ζ basis set, except for the calculation of the energy of the second excited state based on the GS@B3LYP structure, where the GGA and LDA functionals appear to be not well converged with the intermediate basis set (see Supporting Information).

As the above findings suggest, we may select the intermediate basis set (i.e., 6-31+G(d)) as the best compromise to further compare the performance of the 19 different exchange-correlation functionals to the DFT/MRCI results reported in the previous section. Once again, the two geometries corresponding to the optimized ground state (@GS) and the TD-DFT optimized first excited state (@EXC) are used. In Figures 4 and 5, we report the unsigned errors on the excitations energies and oscillator strengths, respectively, of the first three excited states for both structures.

DOI: 10.1021/ct5011246
J. Chem. Theory Comput. 2015, 11, 655−666

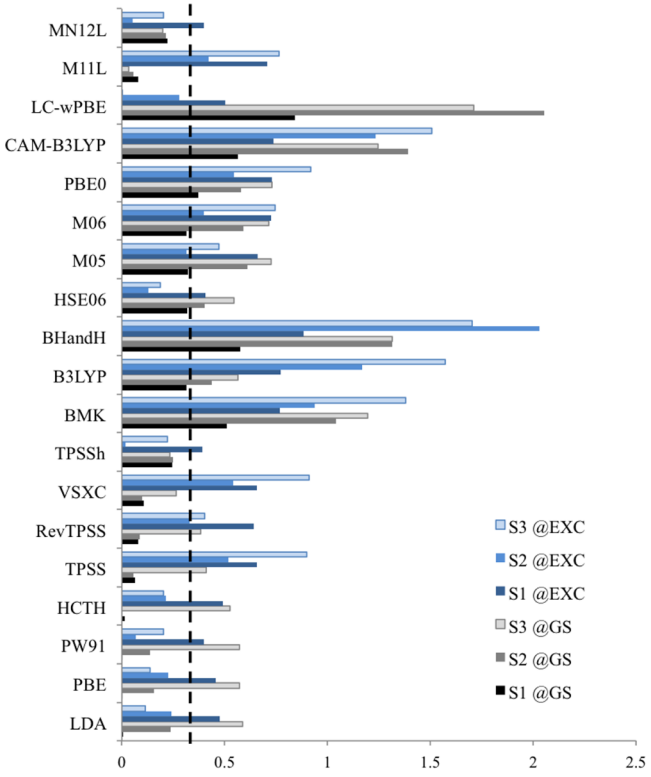

Figure 4. Errors on excitation energies (in eV) of the three lowest excited states of peridinin computed @GS and @EXC using TDA with 19 different density functionals. Errors are computed with respect to DFT/MRCI results. The vertical dashed line indicates the selected threshold (0.3 eV).

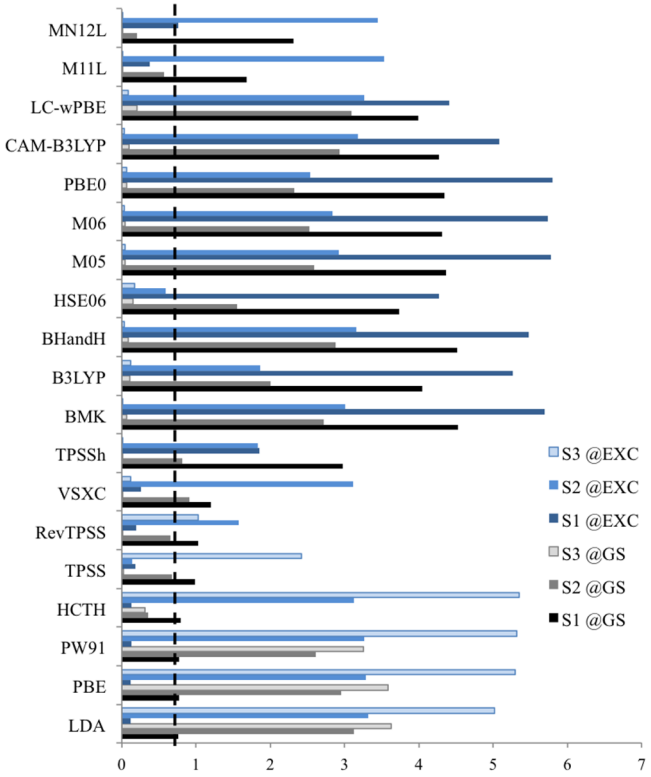

Figure 5. Errors on oscillator strengths (in au) of the lowest three excited states of peridinin computed @GS and @EXC using the TDA with 19 different density functionals. Errors are computed with respect to DFT/MRCI results. The vertical dashed line indicates the selected threshold (0.7 au).

While many functionals are able to provide reasonably accurate predictions of the excitation energies, most functionals fail to reproduce the correct ordering of the excited states, thus presenting large errors with respect to the oscillator strengths of two or more of the considered excited states. This major drawback is strongly related to the well-known inability of TD-DFT to properly characterize the low-lying dark state of Cars.

From a qualitative analysis of the results, it appears that the different functionals can be arranged in terms of their performances into three groups. All the hybrids, even in their long-range corrected versions, perform poorly for most of the quantities of interest, with the exception of TPSSh, which anyway performs worse than its nonhybrid counterpart. GGA and LDA perform reasonably well for excitation energies, but they predict the third state to be the brightest one contrary to the DFT/MRCI results, thus showing poor agreement on the predicted oscillator strengths. The meta-GGAs perform reasonably well both on energies and oscillator strengths.

In order to carry out a more quantitative screening of the functionals, a threshold was set on the allowed errors with respect to four properties of each excited state. In addition to excitation energies and oscillator strengths, the orientation of the transition dipoles was included in this test by considering the angle and the modulus of the distance between the TDA and the DFT/MRCI unsigned transition dipole vectors (considering that we analyze three excited states at two geometries, we have a total of 24 properties in the set). By setting thresholds of 0.3 eV on the excitation energies (dashed line in Figure 4), 0.7 on the oscillator strengths (dashed lines in Figure 5), 3.0 au on the modulus of the difference between transition dipoles, and 2 degrees on the angle between transition dipoles, we were able to identify three main groups.

- Group 1: Long-range hybrids, BMK and BHandH, which can only reproduce 5 or fewer properties with the required accuracy, out of the total 24 properties considered in the test.
- Group 2: Most of the remaining hybrids (B3LYP, PBE0, HSE06) with some hybrid Meta-GGA (M05 and M06), LDA and GGA functionals (PBE and PW91), which can reproduce less than half (i.e., between 6 and 11) of the considered properties with the required accuracy.
- Group 3: Meta-GGA (TPSS, RevTPSS, VSXC, TPSSh, M11L, MN12L) and HCTH, which can reproduce between 12 and 15 of the considered quantities.

Among the six functionals of Group 3, TPSS appears to be the most consistent, while HCTH gives the best results of all quantities but the third excited state, and M11L overestimates (more than the others) the dipole moment of the first excited state. Also for the @EXC geometry, TPSS is the most consistent functional, providing a good description of the three excitation energies and a reasonably good description of the transition dipole of the brightest state (S2). TPSS and RevTPSS find a too bright third state, though, which is not consistent with DFT/MRCI. The correct brightness is only recovered by VSXC and M11L, even though the transition dipoles are definitely overestimated by a factor of 2. Eventually, HCTH fails to find a bright second excited state for the @EXC geometry. It has to be stressed that the @EXC geometry presents a quite different conjugation path with respect to the GS one, being characterized by a much more delocalized

DOI: 10.1021/ct5011246
J. Chem. Theory Comput. 2015, 11, 655−666

structure.[30] This seems to lead to a less accurate description of TDA especially for the second and third states for which the oscillator strengths appear to be not well converged with the chosen basis set and the strength of the third state seems to be transferred to the second one as the basis set size is increased.

Concluding from the above comparison on peridinin, out of the 19 functionals considered, only 3 meta-GGA functionals have been selected to be tested on the whole set of carotenoids, namely TPSS, VSXC, and M11L. For this analysis, only the GS geometry has been used.

The performances of TDA using the three selected functionals are summarized in Figure 6, where the mean

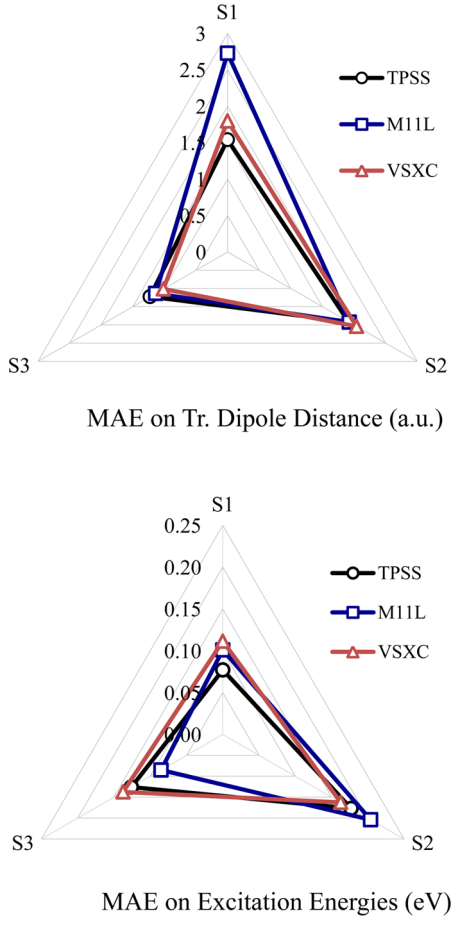

Figure 6. Mean absolute error (MAE) on the transition dipoles (above) and energies (below) for the first three excitations (S1−S2−S3) of the nine Cars. Errors are computed for three functionals (TPSS, M11L, and VSXC) with respect to MRCI/DFT results.

absolute errors, with respect to DFT/MRCI calculations and averaged over the different Cars, are reported (see the Supporting Information for the full set of data).

In general, the behaviors of the different functionals are very similar for the three meta-GGA functionals. M11L shows a better behavior for excitation energies and a slightly worse behavior on transition dipoles. The same conclusion holds for a comparison of the maximum absolute errors (not reported) instead of average errors, confirming the inherent similarity between the different functionals. As the results of TPSS show a slightly larger accuracy for the properties of the S1 state, we decided to use this functional for the further analysis.

5. LIGHT-HARVESTING PROPERTIES

In this section, we present a detailed analysis of the electronic properties (transition energies, transition dipoles, and electronic couplings) determining the description of light-harvesting systems, as obtained with TDA in combination with the selected functional (TPSS) and the reference DFT/MRCI.

In Table 3, we have collected TDA-TPSS excitation energies and oscillator strengths for the nine carotenoids in order of increasing conjugation lengths, whereas in Figure 7 we report a comparison with respect to DFT/MRCI as a function of the conjugation length.

Table 3. TDA-TPSS Excitation Energies and Oscillator Strengths of the Three Lowest Excited States of the Considered Carotenoids Ordered by Increasing Conjugation Length

	S1		S2		S3	
	E (eV)	*f*	*E* (eV)	*f*	*E* (eV)	*f*
peridinin	2.32	1.26	2.59	3.83	2.69	0.03
neoxanthin	2.34	0.19	2.45	5.01	3.08	0.26
violaxanthin	2.28	0.05	2.41	5.37	3.03	0.54
lutein	2.18	0.69	2.34	4.22	2.84	1.07
zeaxanthin	2.11	0.04	2.22	4.32	2.71	0.54
spheroidene	2.08	0.25	2.28	5.34	2.72	0.07
rhodopin-Gl	1.95	0.06	2.11	5.79	2.62	0.89
rhodovibrin	1.84	0.07	2.00	5.86	2.48	0.87
spirilloxanthin	1.74	0.01	1.89	6.02	2.34	0.91

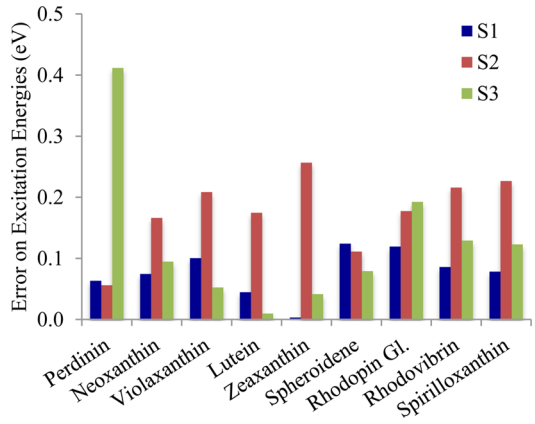

Figure 7. TDA-TPSS errors on transition energies (in eV) with respect to DFT/MRCI as a function of the conjugation length, as reported in Figure 1.

The overall agreement is qualitatively and quantitatively good for the S1 and S3 states with errors oscillating around 0.1 eV (the only evident exception being the S3 state of peridinin for which a much larger error is found). For the bright S2 state a slightly worse picture is found with maximum errors of around 0.2 eV for the longer Cars. The better behavior found for the S1 and S3 states with respect to S2 is an indirect confirmation of what was indicated above concerning the fortuitous cancellation of errors that occurs in the TDA description for states having a non-negligible double excitation character.

A similar comparison can be drawn for the transition dipoles. Table 4 summarizes for the 9 Cars the ratio between TDA and MRCI modules of transition dipoles as well as their orientation

DOI: 10.1021/ct5011246
J. Chem. Theory Comput. 2015, 11, 655−666

Table 4. Ratio of the Modules and Angle between TDA and MRCI Transition Dipole Vectors[a]

	ratio			angle		
	S1	S2	S3	S1	S2	S3
peridinin	2.1	1.1	2.3	0	2	6
neoxanthin	6.9	1.2	2.2	3	1	3
violaxanthin	11.0	1.2	2.1	10	4	2
lutein	11.9	1.1	2.9	9	4	3
zeaxanthin	10.1	1.2	2.7	5	4	4
spheroidene	3.3	1.2	0.8	1	3	6
rhodopin-Gl	10.1	1.3	1.1	2	3	1
rhodovibrin	5.2	1.4	0.8	2	3	1
spirilloxanthin	8.2	1.5	0.6	3	3	1

[a]The reported angles are in degrees.

(here quantified in terms of the angle between the TDA and DFT/MRCI vectors).

The results reported in Table 4 clearly indicate that for all Cars S2 and S3 dipole magnitudes are well reproduced by TDA-TPSS even if the two states present an opposite behavior with respect to the conjugation length: the S2 state is better described for shorter Cars and *vice versa* for the S3 state. For all Cars, a large dipole ratio is found for S1, but we cannot extract a clear trend with the conjugation length. If we focus on the relative orientations between the TDA-TPSS and MRCI dipole vectors, we find an overall good agreement for all states of all Cars with the largest deviations located at the S1 state of the four xanthophylls.

Although it would be tempting to relate the observed errors with the multideterminant nature of the considered states, it is clear by the results summarized in Figure 2 that such a conclusion cannot be drawn for the short-conjugation carotenoids, since the nature of the S1 state shows little dependence on the conjugation length. For the longer carotenoids, on the contrary, it is possible to perform an analysis of the errors in terms of the different percentage of single vs multiple excitations: this analysis is reported in Figure 8.

For these Cars, the absolute error for the S2 state is generally larger than for the S1 and S3 states, even though one would expect that a single reference approach such as TDA should yield a worse description for states dominated by multiple excitations. This apparently unexpected behavior can be explained by noting that the S2 state has a much larger transition dipole, compared to the S1 and S3 states, and the absolute error is consequently larger. However, it is important to note that the error associated with the S2 states decreases as the percentage of single excitation contribution increases, contrary to what is observed for the errors in the S1 and S3 states, which increase as they become more and more dominated by single excitations. All these results seem to further confirm that TDA-TPSS introduces a cancellation of errors, which is very efficient for states with a really significant multideterminant nature. As previously suggested, this can be explained by the fact that when the percentage of multideterminant character of the S1 (and S3) increases the same is true also for the ground state but not for S2.

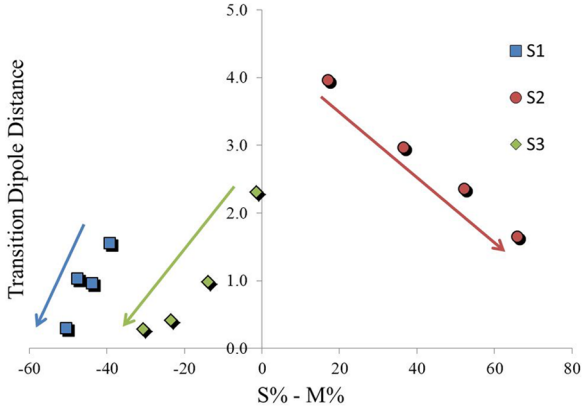

Figure 8. TDA-TPSS transition dipole distances with respect to MRCI/DFT in terms of percentage of single minus multiple excitations for the long Cars (with $N \geq 10$).

Finally, we have studied the performance of TDA-TPSS in describing excitonic couplings between different carotenoids. To calculate the couplings, the transition densities, as computed via DFT/MRCI and TDA-TPSS on the @GS optimized geometries, were decomposed into atomic transition charges (ATCs), using a Mulliken population analysis. ATCs were subsequently placed on atomic crystal-structure coordinates of Cars in selected light-harvesting systems and the excitonic couplings were computed between different excited states of different carotenoids assuming a purely Coulomb interaction among the pigments. We considered the CP29 and LHCII pigment−protein complexes of plant's Photo-System II for calculations involving neoxanthin, lutein, violaxanthin, and zeaxanthin, while the marine algae PCP was selected for calculations involving peridinin.

The results were obtained for structures determined from crystallography, as reported in the Protein Data Bank and modified to include the missing hydrogen atoms. In particular, we used the structure of PCP from ref 72 (PDB ID 1PPR), the structure of CP29 from ref 73 (PDB ID 3PL9), and the structure of LHCII from ref 74 (PDB ID 2BHW). For the sake of clarity, only results obtained on monomers of the PCP and LHCII trimeric proteins are reported in the Tables 5−7. The relative arrangement of the different carotenoids in their corresponding protein environments are visualized for the three systems in Figure 9.

The results obtained for the three LH complexes show a qualitatively good agreement between DFT/MRCI and TDA, whereas, quantitatively, discrepancies appear, which can be related to the differences previously found for the transition dipoles. In particular, although all main couplings are correctly identified by TDA, this approach overestimates most of the largest values (namely those involving the bright S2 state). This effect reflects the TDA overestimation of the S2 transition dipoles reported in Table 4. The large overestimation previously observed for the S1 dipole (see Table 4) is clearly reflected by the too large coupling elements involving this state. The latter effect is particularly evident in the case of highly packed structures such as the monomers of PCP.

Given these overestimations, we can, however, notice that the general agreement is qualitatively good indicating that the shape of the transition densities calculated at the TDA level are similar to the DFT/MRCI ones. This in turn means that a proper picture of the couplings can easily be obtained by a scaling of the transition charges so as to reproduce the MRCI dipoles. This is what is confirmed in Figure 10 where we report the correlation between DFT/MRCI and scaled TDA couplings for all pairs of PID in PCP.

DOI: 10.1021/ct5011246
J. Chem. Theory Comput. 2015, 11, 655−666

Table 5. DFT/MRCI (Left Corner) and TDA-TPSS (Right Corner) Excitonic Couplings among the Eight Peridinin (PID) of the First Monomer of the PCP Light-Harvesting Protein, as Obtained Using Atomic-Transition Charges Placed on Crystal Structure Coordinates[a]

MRCI/DFT \ TDA-TPSS	PID611	PID612	PID613	PID614	PID621	PID622	PID623	PID624
PID611		305 472 42 444 699 60 51 79 7	138 215 21 227 365 34 19 29 3	175 268 29 279 439 47 24 38 4	24 44 3 44 78 6 4 7 1	27 65 5 48 110 9 5 11 1	41 65 6 69 108 10 6 10 1	2 4 0 1 10 0 0 1 0
PID612	51 152 3 162 474 5 8 25 3		186 286 29 291 448 45 27 43 4	90 163 15 132 242 23 12 23 2	26 48 5 61 109 10 6 10 1	179 286 27 283 457 44 28 44 4	143 214 22 223 335 34 21 31 3	0 12 1 6 28 2 1 2 0
PID613	23 68 0 72 213 0 1 2 1	27 83 2 81 248 8 2 6 1		246 502 68 289 611 86 32 60 8	38 65 6 60 103 10 6 9 1	131 208 20 198 313 30 20 31 3	132 205 20 205 316 31 20 31 3	20 43 4 31 66 6 2 6 1
PID614	28 83 3 85 254 9 2 6 1	15 42 1 49 140 2 0 0 0	35 102 2 130 352 18 12 21 6		3 2 1 2 6 0 1 0 0	0 6 0 10 27 2 1 2 0	20 31 2 42 65 6 3 6 1	15 20 2 20 28 3 2 3 0
PID621	5 16 0 16 55 1 0 1 0	6 24 0 20 79 0 0 2 0	6 19 1 19 60 2 0 2 0	0 2 0 1 10 0 0 0 0		275 420 37 424 657 56 47 72 6	136 209 20 227 359 33 19 30 3	170 253 28 277 428 46 25 38 4
PID622	6 19 0 24 78 1 0 2 0	27 84 2 85 256 6 2 7 0	19 56 2 56 169 8 3 10 1	1 6 0 5 23 0 0 0 0	46 144 2 145 448 2 7 24 3		186 285 29 292 448 45 27 42 4	91 165 15 133 244 23 13 23 2
PID623	6 21 0 20 63 1 1 2 0	20 59 3 60 177 10 2 8 1	19 56 3 56 166 10 3 10 1	3 13 0 11 41 1 0 2 0	23 67 0 71 212 0 1 2 1	27 82 3 80 244 9 2 6 1		259 521 69 304 640 90 34 62 8
PID624	0 2 0 3 12 0 0 0 0	1 5 0 6 23 0 0 0 0	3 11 0 13 40 2 0 1 0	2 5 0 5 10 0 0 0 0	28 82 3 82 250 9 2 6 1	15 42 1 50 143 2 0 1 0	37 109 2 138 374 19 11 20 6	

[a]All values are in cm^{-1}.

Table 6. DFT/MRCI (Left Corner) and TDA-TPSS (Right Corner) Excitonic Couplings among the Two Lutein (LUT), One Neoxanthin (NEX), and One Violaxanthin (VIO) of the First Monomer of the LHCII Light-Harvesting Protein, as Obtained Using Atomic-Transition Charges Placed on Crystal Structure Coordinates[a]

MRCI/DFT \ TDA-TPSS	LUT	LUT	NEX	VIO
LUT		13 10 9 7 26 45 10 48 41	3 2 0 16 61 13 15 81 17	2 2 2 9 21 13 5 12 7
LUT	1 5 1 6 56 15 1 14 3		23 143 30 59 378 79 31 198 42	3 61 24 5 119 48 1 35 15
NEX	0 2 1 2 58 16 0 6 2	0 2 0 2 185 32 0 20 3		0 2 1 2 9 4 0 2 1
VIO	0 2 1 1 6 0 0 2 0	0 2 1 6 63 9 1 12 2	0 0 0 0 5 1 0 1 0	

[a]All values are in cm^{-1}.

Table 7. DFT/MRCI (Left Corner) and TDA-TPSS (Right Corner) Excitonic Couplings among One Lutein (LUT), One Neoxanthin (NEX), and One Violaxanthin (VIO) of the CP29 Light-Harvesting Protein, as Obtained Using Atomic-Transition Charges Placed on Crystal Structure Coordinates[a]

MRCI/DFT \ TDA-TPSS	LUT	VIO	NEX
LUT		2 57 28 1 106 54 2 57 27	11 61 12 23 109 20 11 48 9
VIO	0 5 2 9 97 20 2 20 4		5 27 6 62 407 85 19 125 26
NEX	0 3 1 5 72 15 1 8 2	0 2 0 2 186 31 0 20 3	

[a]All values are in cm^{-1}.

6. CONCLUSIONS

In this paper, we have presented a detailed study on the electronic properties of the main carotenoids found in light-harvesting pigment−protein complexes of algae and plants. By using a multireference extension of DFT we have calculated transition properties (energies, dipoles, and densities) for the three lowest singlet excited states of nine different carotenoids. This analysis shows that, in all cases, the lowest state presents a small (but not null) transition dipole which for peridinin becomes significant. We have further shown that a third state, very close in energy to the second bright state, with a significant dipole moment appears for the longest carotenoids. An analysis of single and multiple excitations to these states reveals that, while the S2 state is dominated by single excitations, contributions from multiple excitations are crucial for the first and third excited states. In particular, for the longer Cars, we observe a clear mixing of the S2 and S3 states that explains the decrease of the S3 excitation energy and the parallel increase of

DOI: 10.1021/ct5011246
J. Chem. Theory Comput. 2015, 11, 655−666

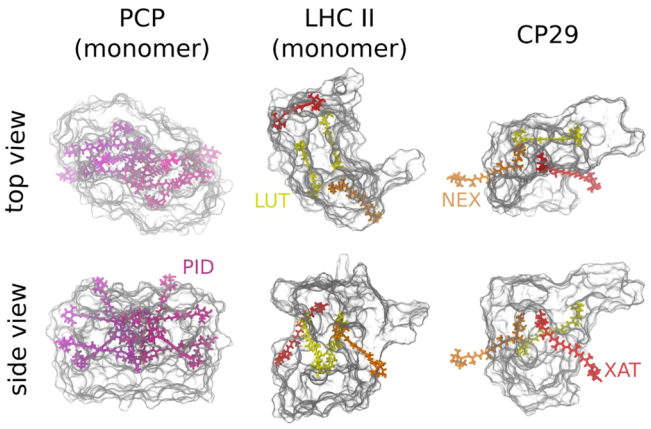

Figure 9. Arrangement of carotenoids in the light-harvesting complexes of PCP (left), LHCII (center), and CP29 (right) proteins, as derived from crystal-structure data. Perdinin (PID, in magenta), lutein (LUT, in yellow), neoxanthin (NEX, in orange), and violaxanthin (XAT, in red) are drawn using the licorice representation, while protein structures are visualized as transparent surfaces.

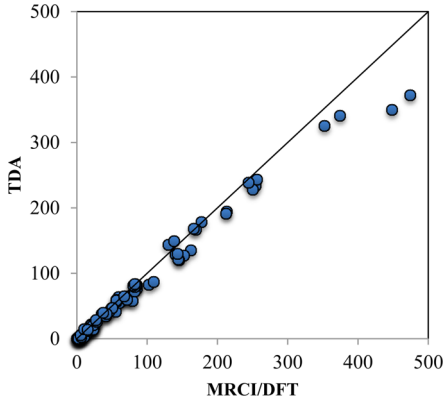

Figure 10. Correlation between TDA-TPSS and DFT/MRCI couplings for all the PID pairs in PCP. The TDA values have been scaled according to the ratio between the involved transition dipoles (see Table 4). All values are in cm^{-1}.

the transition dipole. For the longest Car, spirilloxanthin, S2 and S3 states become almost degenerate with a very similar transition dipole. Using these results as references we have benchmarked the performance of the TDA approach, which for linear all-trans polyenes of increasing length has been previously shown to perform better than TD-DFT. Indeed, we find that for all the investigated carotenoids the combination of TDA with meta-GGA functionals (and in particular TPSS) gives a generally good description of the transition properties of the three states. Our analysis confirms that this behavior is due to cancelation of the effects that the neglect of the multideterminant character has on the ground and the excited states (this also explains why TDA gives a better picture than TDDFT). From our results, it also appears that this cancellation does apply not only to transition energies but also to transition densities and the resulting electronic couplings[75] for which a general good reproduction of the MRCI shape is obtained with TDA. Overall, an efficient yet reasonably accurate computational approach has been defined: this procedure performs reasonably for key parameters relevant for the modeling of energy transfer processes and it could represent an important tool in the description of light-harvesting pigment−protein complexes by means of combined molecular dynamics and quantum-mechanical simulations.

■ ASSOCIATED CONTENT

Supporting Information

Basis set and functional dependence of excitation energies and oscillator strengths of peridinin. Errors on excitation energies and oscillator strengths of the whole set of carotenoids for the three selected meta-GGA functionals, TPSS, VSXC, and M11L. This material is available free of charge via the Internet at http://pubs.acs.org.

■ AUTHOR INFORMATION

Corresponding Authors

*E-mail: oliviero.andreussi@unipi.it.
*E-mail: benedetta.mennucci@unipi.it.

Notes

The authors declare no competing financial interest.

■ ACKNOWLEDGMENTS

O.A. and B.M. acknowledge the European Research Council (ERC) for financial support in the framework of the Starting Grant (EnLight 277755). J.K. thanks the Danish Councils for Independent Research (the Sapere Aude programme).

■ REFERENCES

(1) Polívka, T.; Frank, H. A. Molecular factors controlling photosynthetic light harvesting by carotenoids. *Acc. Chem. Res.* **2010**, *43*, 1125−1134.
(2) Frank, H. A.; Cogdell, R. J. Carotenoids in photosynthesis. *Photochem. Photobiol.* **1996**, *63*, 257−264.
(3) Polívka, T.; Sundström, V. Ultrafast dynamics of carotenoid excited states—From solution to natural and artificial systems. *Chem. Rev.* **2004**, *104*, 2021−2071.
(4) Götze, J. P.; Kröner, D.; Banerjee, S.; Karasulu, B.; Thiel, W. Carotenoids as a shortcut for chlorophyll Soret-to-Q band energy flow. *ChemPhysChem* **2014**, *15*, 3392−3401.
(5) Walla, P. J.; Linden, P. A.; Hsu, C. P.; Scholes, G. D.; Fleming, G. R. Femtosecond dynamics of the forbidden carotenoid S1 state in light-harvesting complexes of purple bacteria observed after two-photon excitation. *Proc. Natl. Acad. Sci. U.S.A.* **2000**, *97*, 10808−10813.
(6) Ruban, A. V.; Johnson, M. P.; Duffy, C. D. P. The photoprotective molecular switch in the photosystem II antenna. *Biochim. Biophys. Acta* **2012**, *1817*, 167−181.
(7) Demmig-Adams, B. Carotenoids and photoprotection in plants: A role for the xanthophyll zeaxanthin. *Biochim. Biophys. Acta, Bioenerg.* **1990**, *1020*, 1−24.
(8) Young, A. J. The photoprotective role of carotenoids in higher plants. *Physiol. Plant.* **1991**, *83*, 702−708.
(9) Scholes, G. D.; Fleming, G. R.; Olaya-Castro, A.; van Grondelle, R. Lessons from nature about solar light harvesting. *Nat. Chem.* **2011**, *3*, 763−774.
(10) Schulten, K. Correlation effects in the spectra of polyenes. *J. Chem. Phys.* **1976**, *64*, 4422.
(11) Tavan, P.; Schulten, K. Electronic excitations in finite and infinite polyenes. *Phys. Rev. B* **1987**, *36*, 4337−4358.
(12) Macpherson, A. N.; Gillbro, T. Solvent dependence of the ultrafast S2 −S1 internal conversion rate of β-carotene. *J. Phys. Chem. A* **1998**, *102*, 5049−5058.
(13) Kopczynski, M.; Ehlers, F.; Lenzer, T.; Oum, K. Evidence for an intramolecular charge transfer state in 12′-apo-β-caroten-12′-al and 8′-apo-β-caroten-8′-al: influence of solvent polarity and temperature. *J. Phys. Chem. A* **2007**, *111*, 5370−5381.
(14) Ehlers, F.; Wild, D. A.; Lenzer, T.; Oum, K. Investigation of the S1/ICT→S0 internal conversion lifetime of 4′-apo-β-caroten-4′-al and

DOI: 10.1021/ct5011246
J. Chem. Theory Comput. 2015, 11, 655−666

8′-apo-β-caroten-8′-al: dependence on conjugation length and solvent polarity. *J. Phys. Chem. A* **2007**, *111*, 2257−2265.
(15) Cerullo, G.; Polli, D.; Lanzani, G.; De Silvestri, S.; Hashimoto, H.; Cogdell, R. J. Photosynthetic light harvesting by carotenoids: Detection of an intermediate excited state. *Science* **2002**, *298*, 2395−2398.
(16) Ostroumov, E. E.; Mulvaney, R. M.; Cogdell, R. J.; Scholes, G. D. Broadband 2D electronic spectroscopy reveals a carotenoid dark state in purple bacteria. *Science* **2013**, *340*, 52−56.
(17) Ostroumov, E.; Müller, M.; Marian, C. M.; Kleinschmidt, M.; Holzwarth, A. Electronic coherence provides a direct proof for energy-level crossing in photoexcited lutein and β-carotene. *Phys. Rev. Lett.* **2009**, *103*, 108302.
(18) Hauer, J.; Maiuri, M.; Viola, D.; Lukes, V.; Henry, S.; Carey, A. M.; Cogdell, R. J.; Cerullo, G.; Polli, D. Explaining the temperature dependence of spirilloxanthin's S* signal by an inhomogeneous ground state model. *J. Phys. Chem. A* **2013**, *117*, 6303−6310.
(19) Polívka, T.; Sundström, V. Dark excited states of carotenoids: Consensus and controversy. *Chem. Phys. Lett.* **2009**, *477*, 1−11.
(20) Schulten, K.; Karplus, M. On the origin of a low-lying forbidden transition in polyenes and related molecules. *Chem. Phys. Lett.* **1972**, *14*, 305−309.
(21) Starcke, J. H.; Wormit, M.; Schirmer, J.; Dreuw, A. How much double excitation character do the lowest excited states of linear polyenes have? *Chem. Phys.* **2006**, *329*, 39−49.
(22) Damjanović, A.; Ritz, T.; Schulten, K. Excitation transfer in the peridinin−chlorophyll−protein of *Amphidinium carterae*. *Biophys. J.* **2000**, *79*, 1695−1705.
(23) Kusumoto, T.; Kosumi, D.; Uragami, C.; Frank, H. A.; Birge, R. R.; Cogdell, R. J.; Hashimoto, H. Femtosecond transient absorption spectroscopic study of a carbonyl-containing carotenoid analogue, 2-(all-trans-retinylidene)-indan-1,3-dione. *J. Phys. Chem. A* **2011**, *115*, 2110−2119.
(24) Macernis, M.; Sulskus, J.; Duffy, C. D. P.; Ruban, A. V.; Valkunas, L. Electronic spectra of structurally deformed lutein. *J. Phys. Chem. A* **2012**, *116*, 9843−9853.
(25) Duffy, C. D. P.; Chmeliov, J.; Macernis, M.; Sulskus, J.; Valkunas, L.; Ruban, A. V. Modeling of fluorescence quenching by lutein in the plant light-harvesting complex LHCII. *J. Phys. Chem. B* **2013**, *117*, 10974−10986.
(26) Hsu, C.-P.; Walla, P. J.; Head-Gordon, M.; Fleming, G. R. The role of the S1 state of carotenoids in photosynthetic energy transfer: The light-harvesting complex II of purple bacteria. *J. Phys. Chem. B* **2001**, *105*, 11016−11025.
(27) Vaswani, H. M.; Hsu, C.-P.; Head-Gordon, M.; Fleming, G. R. Quantum chemical evidence for an intramolecular charge-transfer state in the carotenoid peridinin of peridinin−chlorophyll−protein. *J. Phys. Chem. B* **2003**, *107*, 7940−7946.
(28) Spezia, R.; Zazza, C.; Palma, A.; Amadei, A.; Aschi, M. A DFT study of the low-lying singlet excited states of the all-trans peridinin in vacuo. *J. Phys. Chem. A* **2004**, *108*, 6763−6770.
(29) Grimme, S.; Waletzke, M. A combination of Kohn−Sham density functional theory and multi-reference configuration interaction methods. *J. Chem. Phys.* **1999**, *111*, 5645.
(30) Kleinschmidt, M.; Marian, C. M.; Waletzke, M.; Grimme, S. Parallel multireference configuration interaction calculations on mini-β-carotenes and β-carotene. *J. Chem. Phys.* **2009**, *130*, 044708.
(31) Knecht, S.; Marian, C. M.; Kongsted, J.; Mennucci, B. On the Photophysics of Carotenoids: A Multireference DFT Study of Peridinin. *J. Phys. Chem. B* **2013**, *117*, 13808−13815.
(32) Götze, J. P.; Thiel, W. TD-DFT and DFT/MRCI study of electronic excitations in Violaxanthin and Zeaxanthin. *Chem. Phys.* **2013**, *415*, 247−255.
(33) Marian, C. M.; Kock, S. C.; Hundsdörfer, C.; Martin, H.-D.; Stahl, W.; Ostroumov, E.; Müller, M. G.; Holzwarth, A. R. Spectroscopic properties of phenolic and quinoid carotenoids: A combined theoretical and experimental study. *Photochem. Photobiol. Sci.* **2009**, *8*, 270−278.
(34) Cerón-Carrasco, J. P.; Requena, A.; Marian, C. M. Theoretical study of the low-lying excited states of β-carotene isomers by a multireference configuration interaction method. *Chem. Phys.* **2010**, *373*, 98−103.
(35) Enriquez, M. M.; Hananoki, S.; Hasegawa, S.; Kajikawa, T.; Katsumura, S.; Wagner, N. L.; Birge, R. R.; Frank, H. A. Effect of molecular symmetry on the spectra and dynamics of the intramolecular charge transfer (ICT) state of peridinin. *J. Phys. Chem. B* **2012**, *116*, 10748−10756.
(36) Coccia, E.; Varsano, D.; Guidoni, L. Ab Initio Geometry and Bright Excitation of Carotenoids: Quantum Monte Carlo and Many Body Green's Function Theory Calculations on Peridinin. *J. Chem. Theory Comput.* **2014**, *10*, 501−506.
(37) Eichkorn, K.; Weigend, F.; Treutler, O.; Ahlrichs, R. Auxiliary basis sets for main row atoms and transition metals and their use to approximate Coulomb potentials. *Theor. Chem. Acc.* **1997**, *97*, 119−124.
(38) Lee, C.; Yang, W.; Parr, R. G. Development of the Colle−Salvetti correlation-energy formula into a functional of the electron density. *Phys. Rev. B* **1988**, *37*, 785−789.
(39) Becke, A. Density functional thermochemistry. III: The role of exact exchange. *J. Chem. Phys.* **1993**, *98*, 5648−5652.
(40) *TURBOMOLE V6.3 2011, a development of University of Karlsruhe and Forschungszentrum Karlsruhe GmbH*, 1989−2007, TURBOMOLE GmbH: Karlsruhe, Deutschland; available from http://www.turbomole.com.
(41) Frisch, M. J.; Trucks, G. W.; Schlegel, H. B.; Scuseria, G. E.; Robb, M. A.; Cheeseman, J. R.; Scalmani, G.; Barone, V.; Mennucci, B.; Petersson, G. A.; et al. *Gaussian 09*, Revision A.01; Gaussian Inc: Wallingford, CT, 2009.
(42) Yanai, T.; Tew, D. P.; Handy, N. C. A new hybrid exchange−correlation functional using the Coulomb-attenuating method (CAM-B3LYP). *Chem. Phys. Lett.* **2004**, *393*, 51−57.
(43) Prandi, I. G.; Viani, L.; Mennucci, B. DFT-based classical force-field for carotenoids in the light-harvesting complexes of plants. Submitted **2015**.
(44) Dunning, T. H. Gaussian basis sets for use in correlated molecular calculations. I. The atoms boron through neon and hydrogen. *J. Chem. Phys.* **1989**, *90*, 1007.
(45) Perdew, J. P.; Burke, K.; Ernzerhof, M. Generalized Gradient Approximation Made Simple. *Phys. Rev. Lett.* **1996**, *77*, 3865−3868.
(46) Perdew, J. P.; Burke, K.; Ernzerhof, M. Errata: Generalized gradient approximation made simple. *Phys. Rev. Lett.* **1997**, *78*, 1396−1396.
(47) Perdew, J. P.; Chevary, J.; Vosko, S.; Jackson, K. A.; Pederson, M. R.; Singh, D. J.; Fiolhais, C. Atoms, molecules, solids, and surfaces: Applications of the generalized gradient approximation for exchange and correlation. *Phys. Rev. B* **1992**, *46*, 6671−6687.
(48) Perdew, J.; Chevary, J.; Vosko, S.; Jackson, K.; Pederson, M.; Singh, D.; Fiolhais, C. Erratum: Atoms, molecules, solids, and surfaces: Applications of the generalized gradient approximation for exchange and correlation. *Phys. Rev. B* **1993**, *48*, 4978−4978.
(49) Perdew, J.; Burke, K.; Wang, Y. Generalized gradient approximation for the exchange-correlation hole of a many-electron system. *Phys. Rev. B* **1996**, *54*, 16533−16539.
(50) Perdew, J.; Burke, K.; Wang, Y. Erratum: Generalized gradient approximation for the exchange-correlation hole of a many-electron system [*Phys. Rev. B 54*, 16533 (1996)]. *Phys. Rev. B* **1998**, *57*, 14999−14999.
(51) Hamprecht, F. A.; Cohen, A. J.; Tozer, D. J.; Handy, N. C. Development and assessment of new exchange-correlation functionals. *J. Chem. Phys.* **1998**, *109*, 6264.
(52) Tao, J.; Perdew, J.; Staroverov, V.; Scuseria, G. Climbing the density functional ladder: Nonempirical meta-generalized gradient approximation designed for molecules and solids. *Phys. Rev. Lett.* **2003**, *91*, 146401.
(53) Perdew, J.; Ruzsinszky, A.; Csonka, G.; Constantin, L.; Sun, J. Workhorse semilocal density functional for condensed matter physics and quantum chemistry. *Phys. Rev. Lett.* **2009**, *103*, 026403.

DOI: 10.1021/ct5011246
J. Chem. Theory Comput. 2015, 11, 655−666

(54) Perdew, J. P.; Ruzsinszky, A.; Csonka, G. I.; Constantin, L. A.; Sun, J. Erratum: Workhorse semilocal density functional for condensed matter physics and quantum chemistry [*Phys. Rev. Lett. 103*, 026403 (2009)]. *Phys. Rev. Lett.* **2011**, *106*, 179902.
(55) Van Voorhis, T.; Scuseria, G. E. A novel form for the exchange-correlation energy functional. *J. Chem. Phys.* **1998**, *109*, 400.
(56) Peverati, R.; Truhlar, D. G. M11-L: A local density functional that provides improved accuracy for electronic structure calculations in chemistry and physics. *J. Phys. Chem. Lett.* **2012**, *3*, 117−124.
(57) Peverati, R.; Truhlar, D. G. Performance of the M11 and M11-L density functionals for calculations of electronic excitation energies by adiabatic time-dependent density functional theory. *Phys. Chem. Chem. Phys.* **2012**, *14*, 11363−11370.
(58) Peverati, R.; Truhlar, D. G. An improved and broadly accurate local approximation to the exchange-correlation density functional: The MN12-L functional for electronic structure calculations in chemistry and physics. *Phys. Chem. Chem. Phys.* **2012**, *14*, 13171−13174.
(59) Boese, A. D.; Martin, J. M. L. Development of density functionals for thermochemical kinetics. *J. Chem. Phys.* **2004**, *121*, 3405−3416.
(60) Zhao, Y.; Schultz, N. E.; Truhlar, D. G. Exchange-correlation functional with broad accuracy for metallic and nonmetallic compounds, kinetics, and noncovalent interactions. *J. Chem. Phys.* **2005**, *123*, 161103.
(61) Zhao, Y.; Truhlar, D. G. The M06 suite of density functionals for main group thermochemistry, thermochemical kinetics, noncovalent interactions, excited states, and transition elements: Two new functionals and systematic testing of four M06-class functionals and 12 other function. *Theor. Chem. Acc.* **2007**, *120*, 215−241.
(62) Becke, A. D. A new mixing of Hartree−Fock and local density-functional theories. *J. Chem. Phys.* **1993**, *98*, 1372.
(63) Heyd, J.; Scuseria, G. E.; Ernzerhof, M. Hybrid functionals based on a screened Coulomb potential. *J. Chem. Phys.* **2003**, *118*, 8207.
(64) Heyd, J.; Scuseria, G. E.; Ernzerhof, M. Erratum: "Hybrid functionals based on a screened Coulomb potential" [*J. Chem. Phys. 118*, 8207 (2003)]. *J. Chem. Phys.* **2006**, *124*, 219906.
(65) Heyd, J.; Scuseria, G. E. Efficient hybrid density functional calculations in solids: Assessment of the Heyd−Scuseria−Ernzerhof screened Coulomb hybrid functional. *J. Chem. Phys.* **2004**, *121*, 1187−1192.
(66) Heyd, J.; Scuseria, G. E. Assessment and validation of a screened Coulomb hybrid density functional. *J. Chem. Phys.* **2004**, *120*, 7274−7280.
(67) Heyd, J.; Peralta, J. E.; Scuseria, G. E.; Martin, R. L. Energy band gaps and lattice parameters evaluated with the Heyd−Scuseria−Ernzerhof screened hybrid functional. *J. Chem. Phys.* **2005**, *123*, 174101.
(68) Adamo, C.; Barone, V. Toward reliable density functional methods without adjustable parameters: The PBE0 model. *J. Chem. Phys.* **1999**, *110*, 6158.
(69) Vydrov, O. A.; Heyd, J.; Krukau, A. V.; Scuseria, G. E. Importance of short-range versus long-range Hartree−Fock exchange for the performance of hybrid density functionals. *J. Chem. Phys.* **2006**, *125*, 074106.
(70) Vydrov, O. A.; Scuseria, G. E. Assessment of a long-range corrected hybrid functional. *J. Chem. Phys.* **2006**, *125*, 234109.
(71) Vydrov, O. A.; Scuseria, G. E.; Perdew, J. P. Tests of functionals for systems with fractional electron number. *J. Chem. Phys.* **2007**, *126*, 154109.
(72) Hofmann, E.; Wrench, P. M.; Sharples, F. P.; Hiller, R. G.; Welte, W.; Diederichs, K. Structural basis of light harvesting by carotenoids: Peridinin-chlorophyll-protein from *Amphidinium carterae*. *Science* **1996**, *272*, 1788−1791.
(73) Pan, X.; Li, M.; Wan, T.; Wang, L.; Jia, C.; Hou, Z.; Zhao, X.; Zhang, J.; Chang, W. Structural insights into energy regulation of light-harvesting complex CP29 from spinach. *Nat. Struct. Mol. Biol.* **2011**, *18*, 309−315.
(74) Standfuss, J.; Terwisscha van Scheltinga, A. C.; Lamborghini, M.; Kühlbrandt, W. Mechanisms of photoprotection and non-photochemical quenching in pea light-harvesting complex at 2.5 Å resolution. *EMBO J.* **2005**, *24*, 919−928.
(75) König, C.; Schlüter, N.; Neugebauer, J. Direct determination of exciton couplings from subsystem time-dependent density-functional theory within the Tamm−Dancoff approximation. *J. Chem. Phys.* **2013**, *138*, 034104.

DOI: 10.1021/ct5011246
J. Chem. Theory Comput. 2015, 11, 655−666